in 5 patients and partial response in 34 patients using localized X-ray radiotherapy. The BED_{10} >50 Gy had a significantly better response rate (complete or partial response) of 72.8% compared with 46.7% with BED_{10} ≤50 Gy (p = 0.0299). The present study used BED_{10} >50 Gy in 17 of 18 lesions and showed local control rates of 83% after initial RTRT and 92% at 30 months when we included reirradiation with RTRT for the local relapse. Considering the smaller margin for CTV in RTRT compared with that in radiotherapy without a real-time tracking system, we can say that RTRT can accurately treat liver tumors in motion. The dose specification used in the present study was 80–90% at the periphery of the PTV. More accurate dose specification should be used in future studies.

Treatment of HCC by conventional radiotherapy is difficult owing to the adverse hepatic events that may be caused by radiation. Furuse *et al.* (3) observed Grade 3 toxicity in 18 of 46 patients (39.1%) with HCC within 3 months after radiotherapy of 50 Gy in 5 weeks, and Grade 4 toxicity in 11 of 33 patients (33.3%) thereafter, using an arrangement of two or three coplanar beams. Yang *et al.* (5) found hematologic toxicity in 34.6% and hepatobiliary complications in 26% of 153 patients with HCC treated with radiotherapy. Dawson *et al.* (16) carefully estimated the volume effect of the liver from more than 180 patients and found that RILD was not evident in patients with a mean liver dose of <31 Gy. They estimated that if <25% of the normal liver is treated with radiotherapy, then there may be no upper limit on the dose associated with RILD (17). In their estimation, the liver doses associated with a 5% risk of RILD for uniform irradiation of one third, two thirds, and the whole liver were 90, 47, and 39 Gy, respectively, with a daily dose of 2 Gy. This represents a much larger tolerance in the partial irradiation of the liver compared with whole-liver irradiation. We have seen transient elevation of serum transaminases after liver irradiation, but we have not seen any symptomatic RILD. This absence in our series confirms that the liver can tolerate high-dose partial volume irradiation.

Cheng *et al.* (18) found that HCC patients who were hepatitis B virus carriers or had Child-Pugh Class B cirrhosis presented with a significantly greater susceptibility to radiation-induced liver dysfunction after three-dimensional conformal radiotherapy. Considering that Asian patients with HCC usually suffered from viral hepatitis, dose distribution for the liver is crucial to the preservation of hepatic function. Dawson *et al.* (16) showed that the mean liver doses associated with a 5% risk of classic RILD for primary and metastatic liver cancer are 28 Gy and 32 Gy, respectively, at 2 Gy per fraction. Considering the lower dose tolerance of liver in patients with HCC, RTRT's benefit of reducing irradiation to the normal liver would be more apparent for primary HCC than for metastatic liver cancers.

It is well known that the GI tract is an important serial organ that is at risk in liver irradiation anatomically. In the recent literature, liver irradiation was not associated with serious adverse GI effects. Park *et al.* (14) reported a 5.1% complication rate of localized X-ray therapy for gastric or duodenal ulcer. Yang *et al.* (5) reported that out of 153 patients with HCC treated with radiotherapy, radiation-induced ulcers were found in the stomach (n = 9) and duodenum (n = 14), and bleeding was found in 11 patients (7%), including 1 case of fatal bleeding. We have experienced a single case (1 of 15; 6%) of Grade 3 but transient gastric ulcer; this rate was equivalent to that in the previous series. Yang *et al.* reported 35% hematologic toxicity and 2% pneumonitis. Considering the shorter treatment time and higher daily dose used in the present study, the equivalently low complication rate in our series may be attributable to the high-precision radiotherapy obtained by using RTRT.

Kawashima *et al.* (19) reported on proton treatment for 31 patients with HCC. During a median follow-up period of 31 months (range, 16–54 months), only 1 patient experienced recurrence of the primary tumor, and the 2-year actuarial local progression-free rate was 96% (95% confidence interval [CI] 88%–100%). The actuarial overall survival rate at 2 years was 66% (95% CI 48%–84%). Chiba *et al.* (6) of Tsukuba University reported on 192 HCCs in 162 patients treated with a proton beam at 72 Gy (range, 55–84 Gy) with a follow-up period of 32 months (range, 3–133 months) and found 86.9% local control and 23.5% overall survival at 5 years. Obviously, proton therapy is one of the best solutions using focal radiotherapy in dose distribution. Proton therapy using a real-time tumor-tracking system will become a radical treatment for HCC.

In conclusion, RTRT provided effective focal high doses to liver tumors adjacent to the critical organs or to tumors that are located too deep for other treatments. Because the fiducial markers for RTRT need not be implanted into the tumor itself, RTRT can be applied to HCC in patients who are not candidates for other surgical or nonsurgical treatments.

REFERENCES

1. Gannon CJ, Curley SA. The role of focal liver ablation in the treatment of unresectable primary and secondary malignant liver tumors. *Semin Radiat Oncol* 2005;15:265–272.
2. Liapi E, Hong K, Georgiades CS, *et al.* Three-dimensional rotational angiography: Introduction of an adjunctive tool for successful transarterial chemoembolization. *J Vasc Interv Radiol* 2005;16:1241–1245.
3. Furuse J, Ishii H, Nagase M, *et al.* Adverse hepatic events caused by radiotherapy for advanced hepatocellular carcinoma. *J Gastroenterol Hepatol* 2005;20:1512–1518.
4. Hawkins MA, Dawson LA. Radiation therapy for hepatocellular carcinoma: From palliation to cure. *Cancer* 2006;106:1653–1663.
5. Yang MH, Lee JH, Choi MS, *et al.* Gastrointestinal complications after radiation therapy in patients with hepatocellular carcinoma. *Hepatogastroenterology* 2005;52:1759–1763.
6. Chiba T, Tokuuye K, Matsuzaki Y, *et al.* Proton beam therapy for hepatocellular carcinoma: A retrospective review of 162 patients. *Clin Cancer Res* 2005;11:3799–3805.
7. Kato H, Tsujii H, Miyamoto T, *et al.* Results of the first prospective study of carbon ion radiotherapy for hepatocellular

carcinoma with liver cirrhosis. *Int J Radiat Oncol Biol Phys* 2004;59:1468–1476.
8. Shirato H, Shimizu S, Shimizu T, *et al.* Real-time tumor-tracking radiotherapy. *Lancet* 1999;353:1331–1332.
9. Kitamura K, Shirato H, Shimizu S, *et al.* Registration accuracy and possible migration of internal fiducial gold marker implanted in prostate and liver treated with real-time tumor-tracking radiation therapy (RTRT). *Radiother Oncol* 2002;62: 275–281.
10. Kitamura K, Shirato H, Seppenwoolde Y, *et al.* Tumor location, cirrhosis, and surgical history contribute to tumor movement in the liver, as measured during stereotactic irradiation using a real-time tumor-tracking radiotherapy system. *Int J Radiat Oncol Biol Phys* 2003;56:221–228.
11. Llovet JM, Bru C, Bruix J. Prognosis of hepatocellular carcinoma: The BCLC staging classification. *Semin Liver Dis* 1999;19:329–338.
12. Emami B, Lyman J, Brown A, *et al.* Tolerance of normal tissue to therapeutic irradiation. *Int J Radiat Oncol Bio Phys* 1991;21: 109–122.
13. Couinaud C. Le foie: Études anatomiques et chirurgicales. Paris: Masson; 1957. p. 9–12.
14. Park HC, Seong J, Han KH, *et al.* Dose-response relationship in local radiotherapy for hepatocellular carcinoma. *Int J Radiat Oncol Biol Phys* 2002;54:150–155.
15. Park W, Lim do H, Paik SW, *et al.* Local radiotherapy for patients with unresectable hepatocellular carcinoma. *Int J Radiat Oncol Biol Phys* 2005;61:1143–1150.
16. Dawson LA, Normolle D, Balter JM, *et al.* Analysis of radiation-induced liver disease using the Lyman NTCP model. *Int J Radiat Oncol Biol Phys* 2002;53:810–821.
17. Dawson LA, Ten Haken RK. Partial volume tolerance of the liver to radiation. *Semin Radiat Oncol* 2005;15:279–283.
18. Cheng JC, Wu JK, Lee PC, *et al.* Biologic susceptibility of hepatocellular carcinoma patients treated with radiotherapy to radiation-induced liver disease. *Int J Radiat Oncol Biol Phys* 2004;60:1502–1509.
19. Kawashima M, Furuse J, Nishio T, *et al.* Phase II study of radiotherapy employing proton beam for hepatocellular carcinoma. *J Clin Oncol* 2005;23:1839–1846.

Int J Clin Oncol (2007) 12:8–16
DOI 10.1007/s10147-006-0633-y

REVIEW ARTICLE

Hiroki Shirato · Shinichi Shimizu · Kei Kitamura
Rikiya Onimaru

Organ motion in image-guided radiotherapy: lessons from real-time tumor-tracking radiotherapy

Received: October 31, 2006

Abstract External radiotherapy using imaging technology for patient setup is often called image-guided radiotherapy (IGRT). The most important problem to solve in IGRT is organ motion. Four-dimensional radiotherapy (4DRT), in which the accuracy of localization is improved – not only in space but also in time – in comparison to 3DRT, is required in IGRT. Real-time tumor-tracking radiotherapy (RTRT) has been shown to be feasible for performing 4DRT with the aid of a fiducial marker near the tumor. Lung, liver, prostate, spinal/paraspinal, gynecological, head and neck, esophagus, and pancreas tumors are now ready for dose escalation studies using RTRT.

Key words Image-guided radiotherapy · Real-time tumor-tracking radiotherapy · Gated radiotherapy · Intercepting radiotherapy · Pursuing radiotherapy · Four-dimensional radiotherapy

Introduction

In external radiotherapy, the precise localization of the target volume is the key issue. The development of diagnostic imaging modalities such as computed tomography (CT) and magnetic resonance imaging (MRI) has enabled the performance of three-dimensional conformal radiotherapy (3DCRT) and intensity-modulated radiotherapy (IMRT). For the radiosurgery of intracranial disease, rigid fixation of the skull has been successful in improving the registration of the virtual space during treatment planning in relation to the real space during the actual treatment.[1] For extracranial disease, imaging technology was introduced to guide patient setup in the treatment room.[2] External radiotherapy using imaging technology for patient setup is often called image-guided radiotherapy (IGRT).

H. Shirato (✉) · S. Shimizu · K. Kitamura · R. Onimaru
Division of Radiation Oncology, Department of Radiology, Hokkaido University School of Medicine, North-15 West-7, Kita-ku, 060-8638 Sapporo, Japan
Fax +81-11-706-7876
e-mail: hshirato@radi.med.hokudai.ac.jp

The most important problem in IGRT is organ motion. Organ motion should be taken into account in any IGRT for extracranial diseases. In other words, accuracy in time as well as space is required in IGRT. Four-dimensional radiotherapy (4DRT) is IGRT in which the localization accuracy – not only in space but also in time – is improved in comparison to that in 3DRT. By definition, 4DRT is best performed with a sophisticated IGRT system by which the tumor position is monitored during the delivery of the therapeutic beam. Jiang[3] in a review, pointed out that there is only one system which can monitor the internal position of a tumor during irradiation: the real-time tumor-tracking radiotherapy (RTRT) system developed at Hokkaido University Hospital and made by Mitsubishi Electronics (Tokyo, Japan). As there are already many reviews of IGRT elsewhere, we concentrate in this article on a review of RTRT.

The Japanese Society of Therapeutic Radiology and Oncology (JASTRO) has defined RTRT as external radiotherapy which utilizes real-time tracking technology during the delivery of irradiation. There are two types of RTRT in principle (Fig. 1). One is intercepting irradiation, in which the therapeutic beam is delivered only when the tumor is within the gating window. The other is pursuing irradiation, in which the therapeutic beam is continuously delivered pursuing the position of the tumor. The following review deals with intercepting irradiation for which research started in 1996 at Hokkaido University Hospital.[4]

Lung

Three-dimensional (3D) treatment planning has often been performed while patients breathe freely, with the assumption that the CT images represent the average position of the tumor. Shimizu et al.[5] have investigated the impact of respiratory movement on the free-breathing CT images of small lung tumors using sequential CT scanning with the same table position. Using a preparatory free-breathing CT scan, the patient's couch was fixed at the position where

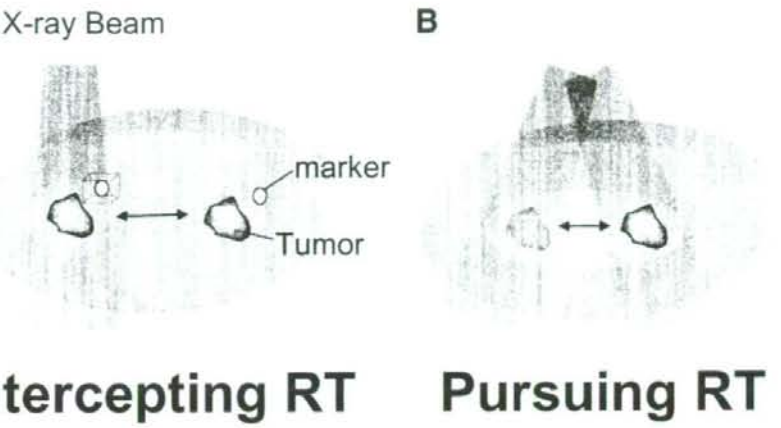

Fig. 1A,B. Two types of real-time tumor-tracking radiotherapy (RTRT). **A** Intercepting irradiation; **B** pursuing irradiation

each tumor showed its maximum diameter on the image. For 16 tumors, over 20 sequential CT images were taken every 2s, with a 1-s acquisition time occurring during free breathing. For each tumor, the distance between the surface of the CT table and the posterior border of the tumor was measured, to determine whether the edge of the tumor was sufficiently included in the planning target volume (PTV) during normal breathing. In the sequential CT scanning, the tumor itself was not visible in the examination slice in 21% (75/357) of cases. There were statistically significant differences between lower-lobe tumors (39.4%; 71/180) and upper-lobe tumors (0%; 0/89; $P < 0.01$) and between lower-lobe tumors and middle-lobe tumors (8.9%; 4/45; $P < 0.01$) in the incidence of the disappearance of the tumor from the image. The mean difference between the maximum and minimum distances between the surface of the CT table and the posterior border of the tumor was 6.4mm (range, 2.1–24.4mm). They concluded that 3D treatment planning for lung carcinoma, without considering organ motion, would significantly underdose many lesions, especially those in the lower lobe.

To achieve precise 3D conformal radiotherapy for mobile tumors, a new radiotherapy system and its treatment planning system were developed and used for clinical practice. Shirato et al.[6] developed a linear accelerator synchronized with a fluoroscopic RTRT system with which the 3D coordinates of a 2.0-mm gold marker in the tumor could be determined every 0.03s. The 3D relationships between the marker and the tumor at different respiratory phases are evaluated using a CT image at each respiratory phase, whereby the optimum phase can be selected to synchronize with irradiation (4D treatment planning). The linear accelerator is triggered to irradiate the tumor only when the marker is located within the region of the planned coordinates relative to the isocenter. The coordinates of the marker were detected with an accuracy of ±1mm during radiotherapy in the phantom experiment. The time delay between recognition of the marker position and the start or stop of megavoltage X-ray irradiation was 0.03s.

The RTRT system consists of four sets of diagnostic X-ray television systems (two of which offer an unobstructed view of the patient at any time), an image processor unit, a gating control unit, and an image display unit.[7] The system recognizes the position of a 2.0-mm gold marker in the human body 30 times per s, using two X-ray television systems. The marker is inserted in or near the tumor, using image-guided implantation. The accuracy of the system and the additional dose due to the diagnostic X-ray were examined in a phantom, and the geometric performance of the system was evaluated in four patients. The phantom experiment demonstrated that the geometric accuracy of the tumor-tracking system was better than 1.5mm for moving targets up to a speed of 40mm/s. The dose due to the diagnostic X-ray monitoring ranged from 0.01% to 1% of the target dose for a 2.0-Gy irradiation of a chest phantom. Shimizu et al.[7] concluded that the RTRT system significantly improved the accuracy of irradiation of targets in motion at the expense of an acceptable amount of diagnostic X-ray exposure.

The RTRT system was useful to analyze the movement of an internal marker. Shimizu et al.[8] investigated the 3D movement of lung tumors through an inserted internal marker, using the RTRT system, and evaluated the efficacy of this system in reducing the internal margin. Four patients with lung cancer were analyzed. A 2.0-mm gold marker was inserted into the tumor. The RTRT system triggered the linear accelerator to irradiate the tumor only when the marker was located within the predetermined "permitted dislocation" of ±1 to ±3mm according to the patient's characteristics. They analyzed 10413–14893 data sets for each of the four patients. The range of marker movement during normal breathing (beam-off period) was compared with that during gated irradiation (beam-on period) by Student's *t*-test. The range of marker movement during the beam-off period was 5.5–10.0mm in the right-left (RL) direction, 6.8–15.9mm in the craniocaudal (CC) direction, and 8.1–14.6mm in the anteroposterior (AP) direction. The range during the beam-on period was reduced to within 5.3mm in

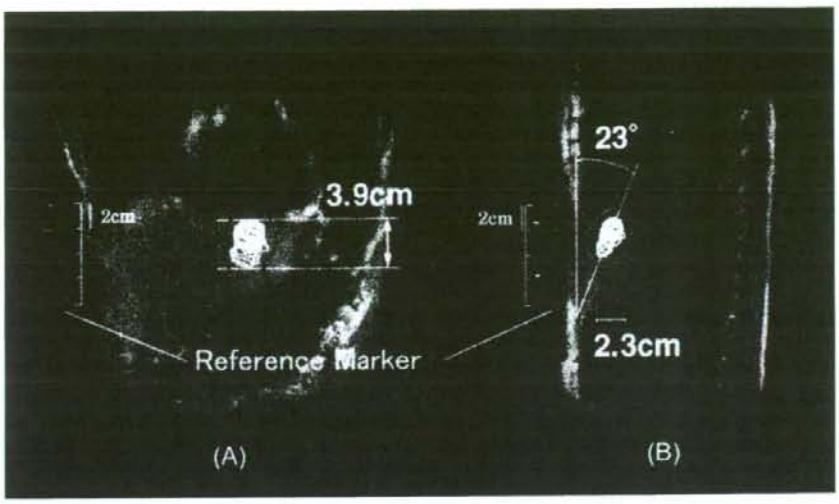

Fig. 2A,B. Four-dimensional (4D) treatment planning, using dynamic magnetic resonance imaging (MRI), for liver cancers. This patient had a liver tumor which had an amplitude of 3.9 cm in the craniocaudal (CC) direction and 2.3 cm in the anteroposterior (AP) direction on dynamic MRI. The internal target volume can be determined by using the summation of sequential images during several respiratory cycles. (From reference 11, with permission)

all directions in all four patients. A significant difference was found between the mean of the range during the beam-off period and the mean of the range during the beam-on period in the RL ($P = 0.007$), CC ($P = 0.025$), and AP ($P = 0.002$) coordinates, respectively. The results of Shimizu et al.[8] showed that treatment with megavoltage X-rays was properly given when the tumor marker moved into the "permitted dislocation" zone from the planned position.

In 2002, Seppenwoolde et al.[9] performed a precise analysis of the behavior of tumor motion in lung tissue to model tumor movement, using the data of 20 patients treated with the RTRT system at Hokkaido University Hospital. The recorded tumor motion was analyzed in terms of the amplitude and curvature of the tumor motion in three directions, the differences in breathing level during treatment, hysteresis (the difference between the inhalation and exhalation trajectory of the tumor), and the amplitude of tumor motion induced by cardiac motion. They confirmed that the average amplitude of the tumor motion was greatest (12 ± 2 mm [SD]) in the CC direction for tumors situated in the lower lobes and not attached to rigid structures such as the chest wall or vertebrae. For the RL and AP directions, tumor motion was small for both upper- and lower-lobe tumors (2 ± 1 mm). The time-averaged tumor position was closer to the exhale position, because the tumor spent more time in the exhalation than in the inhalation phase. The tumor motion was modeled as a sinusoidal movement with varying asymmetry. The tumor position in the exhale phase was more stable than the tumor position in the inhale phase during individual treatment fields. However, in many patients, shifts in the exhale tumor position were observed intra- and interfractionally. These shifts were the result of patient relaxation, gravity (posterior direction), setup errors, and/or patient movement. The 3D trajectory of the tumor showed hysteresis, which ranged from 1 to 5 mm, for 10 of the 21 tumors. The extent of hysteresis and the amplitude of the tumor motion remained fairly constant during the entire treatment. Changes in shape of the trajectory of the tumor were observed between subsequent treatment days for only 1 patient. Fourier analysis revealed that for 7 of the 21 tumors, measurable motion in the range of 1 to 4 mm was caused by the cardiac beat. These tumors were located near the heart or were attached to the aortic arch. The motion due to the heartbeat was greatest in the RL direction. Seppenwoolde et al.[9] suggested that tumor motion due to hysteresis and heartbeat could lower treatment efficiency in gated treatments or could lead to a geographic miss in conventional or active-breathing controlled treatments.

In another study using RTRT, 20 lung tumors in 18 patients were given high-dose hypofractionated focal irradiation (35–48 Gy in 4–8 fractions in 4–10 days) with a planning target volume margin of 5 mm for the tumor.[10] On the whole, 13 (65%) of the 20 tumors were successfully treated with RTRT. Local tumor control was achieved and maintained for all 12 patients (13 tumors) who were treated with RTRT, with a median follow-up of 9 months (range, 5–15 months). Localized radiation pneumonitis was found radiographically in the lung volume that was irradiated with about 20 Gy, and was without symptoms in all but 1 patient. The excellent initial response and low incidence of clinical complications suggest that high-dose hypofractionated focal irradiation, using the RTRT system, could be a good local treatment for peripheral-type lung tumors.

Liver

Four-dimensional (4D) treatment planning using dynamic 3D images was first reported by Shimizu et al.,[11] using not CT but magnetic resonance imaging (MRI; Fig. 2). They investigated the 3D movement of a spherical liver tumor during respiration with MRI, using a high-speed sequence. A marker was placed on the surface of the patient as a distance reference. Repetition time (TR) was 7.7 ms, echo time

(TE) was 4.2 ms, the flip angle was 20°, section thickness was 8 mm, and a 256 × 128 matrix was used. The acquisition time was 1.0 s, followed by an interval of 0.5 s. The 20 tumor contours extracted during 30 s were superimposed on sagittal and coronal MR images. The maximum value of tumor edge location was 3.9 cm in the CC direction, 2.3 cm in the AP direction, and 3.1 cm in the RL direction. The mean length of tumor displacement observed was 2.1 cm in the CC direction, 0.8 cm in the AP, and 0.9 cm in the RL direction. The locus of the center of the tumor contour in the sagittal cross-section was inclined at 23° to the craniocaudal axis of the body, and in the coronal cross-section, this locus was inclined at 18°.

Shimizu et al.[12] have reported that 4D treatment planning has the potential to determine the planning target volume of moving body tumors more precisely than does conventional CT planning. High-speed MRI was applied to the determination of the PTV of moving hepatobiliary tumors. Three moving tumors – two metastatic hepatic tumors and one bile duct tumor – were examined using high-speed MRI and reference fiducial markers before external radiotherapy. Patients were examined for 30 s under conditions of normal breathing during the examination. The coordinates of the center of the tumor contours were shown on sagittal and coronal images displayed on the monitor. The maximum length of movement was 10.6 ± 7.0 mm in the CC direction; 5.2 ± 1.8 mm in the RL direction; and 4.6 ± 1.6 mm in the ventrodorsal direction. When the PTV was determined using MRI in the exhalation phase, with a 10-mm safety margin, the clinical target volume (CTV) was not covered in 19% of all images in the three patients. With MRI in the inhalation phase with a 10-mm safety margin, CTV was not covered in 36% of all images.

Kitamura et al.[13] investigated the 3D intrafractional motion of liver tumors using the RTRT system. Tumor location, cirrhosis, and history of surgery on the liver all had an impact on the intrafractional tumor motion of the liver in the transaxial direction. The data of 20 patients with liver tumors were analyzed. Before treatment, a 2-mm gold marker was implanted near the tumor. Each of the following clinical factors was evaluated to determine its contribution to the amplitude of movement: tumor position, existence of cirrhosis, surgical history, tumor volume, and distance between the isocenter and the marker. The average amplitude of tumor motion in the 20 patients was 4 ± 4 mm (range, 1–12 mm) in the RL direction, 9 ± 5 mm (range, 2–19 mm) in the CC direction, and 5 ± 3 mm (range, 2–12 mm) in the AP direction. The tumor motion of the right lobe was significantly larger than that of the left lobe in the left-right and AP directions ($P = 0.01$). The tumor motion in the left-right and AP directions in the patients with liver cirrhosis was significantly larger than that in the patients without liver cirrhosis ($P < 0.004$). The tumor motion in the left-right and AP directions in the patients who had received a partial hepatectomy was significantly smaller than that in the patients who had no history of any operation on the liver ($P < 0.03$). Thus, three of the five clinical factors examined (i.e., tumor position in the liver, cirrhosis, and history of surgery on the liver) significantly affected the tumor motion of the liver in the transaxial direction during stereotactic irradiation. Frequency analysis revealed that for 9 (45%) of the 20 tumors, the cardiac beat caused measurable motion. The 3D trajectory of the tumor showed hysteresis for 4 (20%) of the 20 tumors. The average treatment efficiency of RTRT was 40%.

Prostate motion

Shimizu et al.[14] have shown that the implantation of fiducial markers and the RTRT system can reduce uncertainty due to setup error and internal organ motion in the precise localization and verification of prostate and bladder cancers. The position of the patient can be corrected by adjusting the actual marker position to the planned marker position, which has been transferred from the 3D radiation treatment planning system and superimposed on the fluoroscopic image on the display unit of the RTRT system. Ten patients with prostate cancer and 5 patients with bladder cancer were examined for the treatment setup on 91 occasions. After manual setup using skin markers, the median absolute value of discrepancies between the actual position of the marker and the planned position of the marker for prostate cancer was 3.4 mm (range, 0.1–8.9 mm), 4.1 mm (range, 0.2–18.1 mm), and 2.3 mm (range, 0.0–10.6 mm) for the RL, AP, and CC directions, respectively. The 3D median distance between the actual and planned positions of the marker was 6.9 mm (range, 1.1–18.2 mm) for prostate cancer and 6.9 mm (range, 1.7–18.6 mm) for bladder cancer. After relocation using RTRT, the 3D distance between the actual and planned position of the marker was 0.9 ± 0.9 mm. Median 3D distances between actual positions for the marker after treatment delivery and planned positions during daily radiotherapy were 1.6 mm (range, 0.0–6.3 mm) and 2.0 mm (range, 0.5–8.0 mm) in patients with prostate cancer and bladder cancer, respectively.

Kitamura et al.[15] quantified 3D movement of the prostate gland with the patient in the supine and prone positions to analyze the movement frequency for each treatment position. In ten patients, the coordinates of the gold marker were recorded every 0.033 s for 2 min during RTRT with the patient in the supine treatment position. The patient was then moved to the prone position, and the marker was tracked for 2 min to acquire data regarding movement in this position. Measurements were taken five times for each patient (once a week); a total of 50 sets for the ten patients were analyzed. Discrete Fourier transform of the unfiltered data was performed for the frequency analysis of prostate movement. No apparent difference in movement was found among individuals. The amplitude of 3D movement was 0.1–2.7 mm in the supine and 0.4–24 mm in the prone position. The amplitude in the supine position was significantly smaller in all directions than that in the prone position ($P < 0.0001$). The amplitude in the CC and AP directions was larger than that in the RL direction in the prone position ($P < 0.0001$). No characteristic movement frequency was detected in the supine position. The respiratory fre-

quency was detected for all patients in the prone position regarding movement in the CC and AP directions. The results of the frequency analysis suggest that, in the prone position, prostate movement is affected by the respiratory cycle and is influenced by bowel movement. The results of this study have confirmed that, in the treatment of prostate cancer, internal organ motion is less frequent in the supine position than in the prone position. RTRT was suggested to be useful in reducing uncertainty due to the effects of the respiratory cycle, especially with patients in the prone position.

Early clinical results using the RTRT system and forward IMRT were reported by Kitamura et al.[16] Patients were classified into prognostic risk groups on the basis of the presence of pretreatment prostate-specific antigen, clinical stage, and histologic differentiation. Neoadjuvant hormonal therapy was administered to patients in the high-risk group for 6 months before radiation therapy commenced. The radiation dose was escalated in increments of 5 Gy from 65 Gy, using a daily dose of 2.5 Gy (65 Gy/2.5 Gy), following the dose-escalation rules. Acute and late gastrointestinal and genitourinary morbidities due to radiation therapy were scored according to the toxicity criteria of the Radiation Therapy Oncology Group (RTOG)/European Organization for Research and Treatment of Cancer. Eighteen patients were classified as being in the high-risk group. The total dose was escalated, with 65 Gy/2.5 Gy being administered to 12 patients and 70 Gy/2.5 Gy to 19 patients. The median follow-up period was 37 months (range, 30–43 months) for the 65-Gy arm, and 19 months (range, 10–27 months) for the 70-Gy arm. Patients in the 65-Gy/2.5-Gy arm experienced no acute toxicity and grade 1 late gastrointestinal toxicity (8.3%). Patients in the 70-Gy/2.5-Gy arm experienced grade 1 acute gastrointestinal toxicity (5.3%) and grade 1 and 2 acute genitourinary toxicities (15.8%). In this study period, no patients experienced dose-limiting toxicity (defined as a grade 3 or higher acute toxicity) or a grade 2 or higher late complication. One prostate-specific antigen relapse was observed in the 65-Gy arm and two prostate-specific antigen relapses were observed in the 70-Gy arm. Up to 70 Gy/2.5 Gy IMRT – equivalent to 80 Gy with a daily dose of 2.0 Gy – assuming an alpha/beta ratio of 1.5 – assisted by the RTRT system, was administered safely with a reasonable biochemical control rate.

Spinal schwannoma

The efficacy of the RTRT system, using three gold markers for estimating translational error, rotational setup error, and the dose to normal structures, was tested in five patients with spinal schwannoma, and a phantom.[17] Translational error was calculated by comparing the actual position of the marker closest to the tumor to its planned position, and the rotational setup error was calculated using the three markers around the target. Theoretically, the actual coordinates can be adjusted to the planning coordinates by sequential rotation of gamma° around the AP axis, beta° around the CC axis, and alpha° around the RL axis, in this order. We measured the accuracy of the rotational calculation using a phantom. Five patients with spinal schwannoma located at a minimum of 1–5 mm from the spinal cord were treated with RTRT. Three markers were inserted percutaneously into the paravertebral deep muscle in three patients and surgically into two consecutive vertebral bones in the two other patients. In the phantom study, the mean discrepancy between the actual and calculated rotational error was –0.1 ± 0.5°. The random error of rotation was 5.9°, 4.6°, and 3.1° for alpha, beta, and gamma, respectively. The systematic error was 7.1°, 6.6°, and 3.0° for alpha, beta, and gamma, respectively. The mean rotational setup error (0.2 ± 2.2°, –1.3 ± 2.9°, and –1.3 ± 1.7° for alpha, beta, and gamma, respectively) in the two patients for whom surgical marker implantation was used was significantly smaller than that in the three patients for whom percutaneous insertion was used (6.0 ± 8.2°, 2.7 ± 5.9°, and –2.1 ± 4.6° for alpha, beta, and gamma). Random translational setup error was significantly reduced by the RTRT setup ($P < 0.0001$). Systematic setup error was significantly reduced by the RTRT setup only in those patients who received surgical implantation of the marker ($P < 0.0001$). The maximum dose to the spinal cord was estimated to be 40.6–50.3 Gy after consideration of the rotational setup error, vs a planned maximum dose of 22.4–51.6 Gy. Surgical implantation of the marker into the vertebral bone was shown to be sufficiently rigid for the calculation of the rotational setup error. Fractionated radiotherapy for spinal schwannoma using the RTRT system may well be an alternative or supplement to surgical treatment.

Gynecological malignancies

The feasibility and accuracy of high-dose 3D conformal boost (3DCB), using three internal fiducial markers and a two-orthogonal X-ray setup of the RTRT system in patients with gynecological malignancies, were investigated in ten patients by Yamamoto et al.[18] The SD of the distribution of systematic deviations (Σ) was reduced from 3.8, 4.6, and 4.9 mm for the three markers in the manual setup to 2.3, 2.3, and 2.7 mm in the setup using the internal markers. The average SD of the distribution of random deviations (sigma) was reduced from 3.7, 5.0, and 4.5 mm for the three markers in the manual setup to 3.3, 3.0, and 4.2 mm in the marker setup. The appropriate PTV margin was estimated to be 10.2, 12.8, and 12.9 mm for the three markers in the manual setup and 6.9, 6.7, and 8.3 mm in the gold marker setup, using the formula 2Σ + 0.7 sigma. The setup of patients with three markers and a two-orthogonal X-ray is useful to reduce the PTV margin and to perform 3DCB.

Esophagus

Hashimoto et al.[19] evaluated the feasibility of real-time monitoring of a fiducial marker in/near the digestive tract

to analyze the motion of organs at risk to determine a reasonable internal margin. They developed two methods to insert a fiducial marker into/near the digestive tract adjacent to the target volume. One method involved an intraoperative insertion technique, and the other involved endoscopic insertion into the submucosal layer of the normal digestive tract. Fourteen markers (2 in the mediastinum and 12 in the abdomen) were implanted intraoperatively in 14 patients with no apparent migration. Seventeen of 20 markers (13/14 in the esophagus, 1/2 in the stomach, and 3/4 in the duodenum) were implanted in 18 patients, using endoscopy, without dropping. No symptomatic adverse effects related to insertion were observed. The mean/SD values for the range of motion of the esophagus were 3.5/1.8, 8.3/3.8, and 4.0/2.6 mm for the RL, CC, and AP directions, respectively, in patients with intrafractional tumor motion less than 1.0 cm. They concluded that both the intraoperative and the endoscopic insertions of a fiducial marker into/near the digestive tract for the monitoring of organs at risk were feasible, and the margin for internal motion could be individualized using the RTRT system.

Head and neck

To reduce setup error and intrafractional movement in head-and-neck treatment, gold markers implanted in a mouthpiece were used in RTRT by Oita et al.[20] Three 2-mm gold markers were implanted into a mouthpiece that had been custom made for each patient before the treatment planning process. Setup errors in the conventional immobilization system using the shell (manual setup) and the RTRT system (RTRT setup) were compared. Eight patients with pharyngeal tumors were enrolled. The systematic setup errors were 1.8, 1.6, and 1.1 mm in the manual setup and 0.2, 0.3, and 0.3 mm in the RTRT setup in the RL, CC, and AP directions, respectively. Statistically significant differences were observed with respect to the variances in setup error ($P < 0.001$). The systematic and random intrafractional errors were maintained within the ranges of 0.2–0.6 mm and 1.0–2.0 mm, respectively. The rotational systematic and random intrafractional errors were estimated to be 2.2–3.2° and 1.5–1.6°, respectively. Oita et al.[20] concluded that the setup error and planning target volume margin could be significantly reduced using an RTRT system with a mouthpiece and three gold markers.

Pancreas

Ahn et al.[21] have reported the usage of RTRT for unresectable pancreatic cancer. Three patients were treated with intraoperative electron-beam radiation therapy, at the time of open biopsy, and postoperative external-beam radiation therapy, using an RTRT system with a 2.0-mm diameter gold ball implanted into the pancreas. The total BED alpha/beta = 10 was intended to be equivalent to that of delivering 60 Gy by 2.0 Gy/fraction, while the actual dose schedules were individualized. During the RTRT course, the average movements of markers in the RL, CC, and AP directions were 3.0 mm (range, 1.7–5.2 mm), 5.2 mm (range, 3.5–6.8 mm), and 3.5 mm (range, 2.7–5.1 mm), respectively. During and after the course of postoperative radiation therapy, no acute side effects of RTOG grade II or higher were detected. The objective tumor responses, as evaluated by CT scans 3 months after the treatment, were two partial responses, and no response in one patient. Using the RTRT technique, the margin of treatment planning and the possible errors in target localization were reduced, and the 3D movement of the internal marker implanted in the pancreas was able to be analyzed.

Fiducial markers

The registration accuracy and possible migration of internal fiducial gold markers implanted into liver and prostate were investigated by Kitamura et al.[22] Internal fiducial gold markers were implanted in 14 patients with prostate cancer and 4 patients with liver tumors. Computed tomography (CT) was carried out as part of the treatment planning in these 18 patients. A total of 72 follow-up CT scans were taken. Kitamura et al.[22] calculated the relative relationship between the coordinates of the center of the mass (CM) of the organs and those of the marker. A discrepancy in the CM coordinates during a follow-up CT compared to those recorded during the planning CT was used to study possible marker migration. The SD of interobserver variations in the CM coordinates was within 2.0 mm and within 0.4 mm for the organ and the marker, respectively, in seven observers. Assuming that organs do not shrink, grow, or rotate, the maximum SD of migration error in each direction was estimated to be less than 2.5 mm for the liver and less than 2.0 mm for the prostate. Most of the marker movement could be attributed to measurement uncertainty, which also influences registration in actual treatment planning. Thus, these authors concluded that even with a gold marker and the RTRT system, a reasonable amount of PTV margin should be used to take into account registration uncertainty.

Equipment and techniques for the insertion of 2.0-mm-diameter gold markers into or near a tumor were improved to take into account rotational error and migration of the markers.[23] Three markers were used to adjust the CM of the target volume to the planned position in spinal/paraspinal lesions and prostate tumors (three-marker method). The feasibility of the marker insertion and the stability of the marker positions were tested using stopping rules in the clinical protocol (i.e., the procedure was abandoned if two of three or three of six patients experienced marker dropping or migration). After evaluation of the feasibility, the stability of the marker positions was monitored in those patients who entered the dose-escalation study. Each of

the following was shown to be feasible: bronchoscopic insertion for the peripheral lung; image-guided transcutaneous insertion for the liver; cystoscopic and image-guided percutaneous insertion for the prostate; and surgical implantation for spinal/paraspinal lesions. Transcutaneous insertion of markers for spinal/paraspinal lesions and bronchoscopic insertion for central lung lesions were abandoned. Overall, marker implantation was successful and was used for real-time tumor tracking in RT in 90 (90%) of 100 lesions. No serious complications related to the marker insertion were noted for any of the 100 lesions. Using three markers surgically implanted into the vertebral bone, the mean ± SD in distance among the three markers was within 0.2 ± 0.6 mm (range, −1.4 to 0.8 mm) throughout the treatment period of 30 days. The distance between the three markers gradually decreased during RT in five of six prostate cancers, consistent with a mean rate of volume regression of 9.3% (range, 0.015%–13%) in 10 days. The three-marker method has been shown to be a useful technique for precise setup for spinal/paraspinal lesions and prostate tumors.

The fixation rate of markers using the bronchial insertion technique, the reliability of the setup using markers around the target volume, dislocation of the markers after RTRT, and the long-term toxicity of marker insertion were investigated recently.[24] Between July 2000 and April 2004, 154 gold markers were inserted into 57 patients with peripheral lung cancer. The distances between the implanted markers in 198 measurements in 71 set-ups in 11 patients were measured using two sets of orthogonal diagnostic X-ray images of the RTRT system. The distance between the markers and the chest wall was also measured in a transaxial CT image on 186 occasions in 48 patients during treatment planning and during follow-up. The median treatment time was 6 days (range, 4–14 days). In 115 (75%) of the 154 inserted markers, the gold marker was detected throughout the treatment period. Of 122 markers detected at CT planning, 115 (94%) were detected until the end of treatment. The variation in the distances between the implanted markers was within ±2 mm in 95% and within ±1 mm in 80% during treatment. The variation in the distances between the implanted markers was more than 2 mm in at least one direction in 9% of the setups for which reexamination with a CT scan was indicated. The fixation rate in the left upper lobe was lower than that in the other lobes. A statistically significant relationship was found between a shorter distance between the markers and the chest wall and the fixation rate, suggesting that the markers in the smaller bronchial lumens fixed better than those in the larger lumens. A learning curve among the endoscopists was suggested in regard to the fixation rate. The distance between the markers and the chest wall changed significantly within a median of 44 days (range, 16–181 days) after treatment. The fixation of markers into the bronchial tree was useful for setup for peripheral lung cancer and had an accuracy of ±2 mm during the 1- to 2-week treatment period. The relationship between the markers and tumor can change significantly after 2 weeks, suggesting that adaptive 4DRT is required.

3D Conformal setup, 4D setup, and external surrogate

Shirato et al.[25] have made a system correcting for the rotational error of the target without having to reposition the patient, using three fiducial markers and two orthogonal fluoroscopic images. They called this system "three-dimensional conformal setup" (3D-CSU) and have reported its usefulness. The rotation angles (alpha, beta, gamma) of the coordinates of the actual CTV relative to the planned CTV are calculated around the RL (x), CC (y), and AP (z) axes of the planned CTV. The angles of the gantry head, collimator, and linear accelerator treatment couch are adjusted according to the rotation of the actual coordinates of the tumor in relation to the planned coordinates. The center of gravity of the phantom was corrected within 0.9 ± 0.3 mm (mean ± SD), 0.4 ± 0.2 mm, and 0.6 ± 0.2 mm for the rotation of the phantom from 0–30° around the RL, CC, and AP axes, respectively, every 5°. Dose distribution was shown to be consistent with the planned dose distribution every 10° of the rotation from 0° to 30°. The mean rotational error after 3D-CSU was −0.4 ± 0.4° (mean ± SD), −0.2 ± 0.4°, and 0.0 ± 0.5° around the RL, CC, and AP axes, respectively, for rotation from 0° to 90°. Phantom studies showed that 3D-CSU was useful for performing rotational correction of the target volume without correcting the position of the patient on the treatment couch. Shirato et al.[25] concluded that 3D-CSU would be clinically useful for paraspinal tumors and prostate cancers in regions not subject to large internal organ motion.

In 2005, Shirato et al.[26] developed a 4D setup system using a new RTRT system to reduce the uncertainty of registration for lung tumors. During treatment planning and daily setup in the treatment room, the trajectory of the internal fiducial marker was recorded for 1 to 2 min at the rate of 30 times per s. To maximize gating efficiency, the patient's position on the treatment couch was adjusted using the 4D setup system with fine online remote control of the treatment couch. The trajectory of the marker detected in the 4D setup system was well visualized and was used for daily setup (Fig. 3). Various degrees of interfractional and intrafractional changes in the absolute amplitude and speed of the internal marker were detected. Readjustments were necessary during each treatment session, prompted by baseline shifting of the tumor position. The 4D setup system was shown to be useful for reducing the uncertainty of tumor motion and for increasing the efficiency of gated irradiation. Considering the interfractional and intrafractional changes in speed and amplitude detected in this study, Shirato et al.[26] concluded that intercepting radiotherapy using the RTRT system was a safe and cost-effective method for 4DRT.

To mitigate motion-induced irradiation of normal lung tissue, clinics have employed external markers to gate the treatment beam. This technique assumes that the correlation between the external surface and the internal tumor position remains constant interfractionally and intrafractionally. Berbeco et al.[27] assessed the validity of this assumption of correlation for external surface-based gated

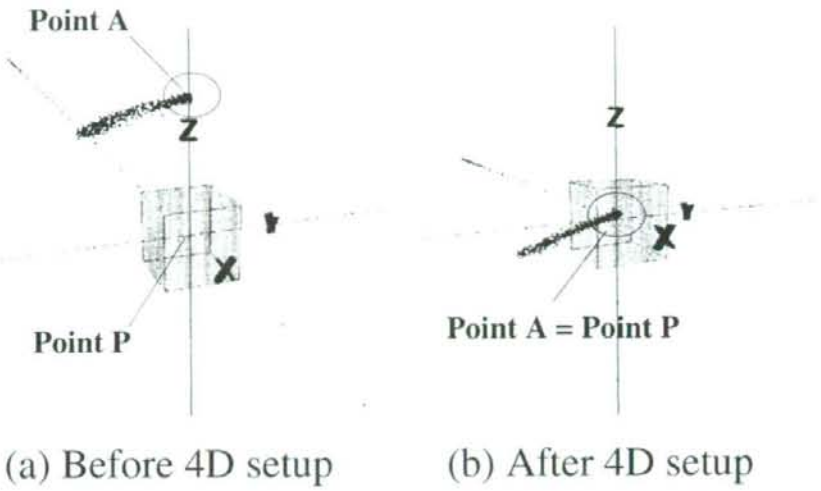

Fig. 3. Trajectory of a marker near a lung tumor in a patient with lung cancer before and after four-dimensional setup. Each spot corresponds to the position of the marker as detected by the real-time tumor-tracking radiotherapy system. In this case, Point P and the gating window (box) were set at the isocenter with 2 mm isotropical "permitted dislocation" from Point P. The actual position of the marker at the end of expiration, Point A, in the trajectory of the marker is adjusted to Point P by moving the treatment couch. The *x*, *y* and *z* are consistent with the right-left, craniocaudal, and anteroposterior directions, respectively

radiotherapy, by measuring the residual tumor motion within a gating window. Eight patients with lung tumors with implanted fiducial markers were studied at the NTT Hospital in Sapporo, Japan. Synchronized internal marker positions and external abdominal surface positions were measured during the entire course of treatment. Both amplitude- and phase-based gating methods were investigated. For each method, three gating windows were investigated, each giving a 40%, 30%, and 20% duty cycle, respectively. The residual motion of the internal marker within these six gating windows was calculated. The beam-to-beam variation and day-to-day variation in the residual motion were calculated for both gating modalities. Berbeco et al.[27] found that the residual motion (95th percentile) was between 0.7 and 5.8 mm, 0.8 and 6.0 mm, and 0.9 and 6.2 mm for the 20%, 30%, and 40% duty cycle windows, respectively. Five of the eight patients showed less residual motion with amplitude-based gating than with phase-based gating. Large fluctuations (>300%) were seen in the residual motion between some beams. Overall, the mean beam-to-beam variation from the previous treatment beam was 37% for amplitude-based gating and 42% for phase-based gating. The day-to-day variation from the previous day was 29% for amplitude-based gating and 34% for phase-based gating. Although gating reduced the total tumor motion, the residual motion behaved unpredictably. Residual motion during treatment could exceed that which might have been considered in the treatment plan. Treatment margins that take motion into account should be individualized, and daily imaging should be performed to ensure that the residual motion does not exceed the planned motion on a given day.

Concluding remarks

The benefit of the RTRT system in reducing the uncertainty in regard to setup and organ motion has been shown in the actual treatment of patients. Reports of the benefits of the RTRT system in improving the clinical outcome of RT have begun to be published recently, 5–7 years after the start of clinical trials. Several studies have shown that a predictive model of respiration may be useful to reduce the requirement for fluoroscopic monitoring during irradiation.[28] However, any risk of missing the CTV from the PTV must be avoided. We need to be careful about the residual error due to organ motion, which often cannot be predicted in IGRT.[29] Image is better than imagination, but an image is always different from the real.

References

1. Aoyama H, Shirato H, Tago M, et al. (2006) Stereotactic radiosurgery plus whole-brain radiation therapy vs stereotactic radiosurgery alone for treatment of brain metastases: a randomized controlled trial. JAMA 295:2483–2491
2. Uematsu M, Shioda A, Tahara K, et al. (1998) Focal, high dose, and fractionated modified stereotactic radiation therapy for lung carcinoma patients: a preliminary experience. Cancer 82:1062–1070
3. Jiang SB (2006) Technical aspects of image-guided respiration-gated radiation therapy. Med Dosim 31:141–151
4. Shirato H, Shimizu S, Shimizu T, et al. (1999) Real-time tumor-tracking radiotherapy. Lancet 353:1331–1332
5. Shimizu S, Shirato H, Kagei K, et al. (2000) Impact of respiratory movement on the computed tomographic images of small lung tumors in three-dimensional (3D) radiotherapy. Int J Radiat Oncol Biol Phys 46:1127–1133
6. Shirato H, Shimizu S, Kitamura K, et al. (2000) Four-dimensional treatment planning and fluoroscopic real-time tumor tracking radiotherapy for moving tumor. Int J Radiat Oncol Biol Phys 48:435–442
7. Shirato H, Shimizu S, Kunieda T, et al. (2000) Physical aspects of a real-time tumor-tracking system for gated radiotherapy. Int J Radiat Oncol Biol Phys 48:1187–1195
8. Shimizu S, Shirato H, Ogura S, et al. (2001) Detection of lung tumor movement in real-time tumor-tracking radiotherapy. Int J Radiat Oncol Biol Phys 51:304–310
9. Seppenwoolde Y, Shirato H, Kitamura Y, et al. (2002) Precise and real-time measurement of 3D tumor motion in lung due to breathing and heartbeat, measured during radiotherapy. Int J Radiat Oncol Biol Phys 53:822–834

10. Harada T, Shirato H, Obura S, et al. (2002) Real-time tumor-tracking radiation therapy for lung carcinoma by the aid of insertion of a gold marker using bronchofiberscopy. Cancer 95:1720–1727
11. Shimizu S, Shirato H, Xo B, et al. (1999) Three-dimensional movement of a liver tumor detected by high-speed magnetic resonance imaging. Radiother Oncol 50:367–370
12. Shimizu S, Shirato H, Aoyama H, et al. (2000) High-speed magnetic resonance imaging for four-dimensional treatment planning of conformal radiotherapy of moving body tumors. Int J Radiat Oncol Biol Phys 48:471–474
13. Kitamura K, Shirato H, Seppenwoolde Y, et al. (2003) Tumor location, cirrhosis, and surgical history contribute to tumor movement in the liver, as measured during stereotactic irradiation using a real-time tumor-tracking radiotherapy system. Int J Radiat Oncol Biol Phys 56:221–228
14. Shimizu S, Shirato H, Kitamura K, et al. (2000) Use of an implanted marker and real-time tracking of the marker for the positioning of prostate and bladder cancers. Int J Radiat Oncol Biol Phys 48:1591–1597
15. Kitamura Y, Shirato H, Seppenwoolde Y, et al. (2002) Three-dimensional intrafractional movement of prostate measured during real-time tumor-tracking radiotherapy in supine and prone treatment positions. Int J Radiat Oncol Biol Phys 53:1117–1123
16. Kitamura K, Shirato H, Shinohara N, et al. (2003) Reduction in acute morbidity using hypofractionated intensity-modulated radiation therapy assisted with a fluoroscopic real-time tumor-tracking system for prostate cancer: preliminary results of a phase I/II study. Cancer J 9:268–276
17. Onimaru R, Shirato H, Aoyama H, et al. (2002) Calculation of rotational setup error using the real-time tracking radiation therapy (RTRT) system and its application to the treatment of spinal schwannoma. Int J Radiat Oncol Biol Phys 54:939–947
18. Yamamoto R, Yonesaka a, Nishioka S, et al. (2004) High dose three-dimensional conformal boost (3DCB) using an orthogonal diagnostic X-ray set-up for patients with gynecological malignancy: a new application of real-time tumor-tracking system. Radiother Oncol 73:219–222
19. Hashimoto K, Shirato H, Katoh M, et al. (2005) Real-time monitoring of a digestive tract marker to reduce adverse effects of moving organs at risk (OAR) in radiotherapy for thoracic and abdominal tumors. Int J Radiat Oncol Biol Phys 61:1559–1564
20. Oita S, Ohmori K, Obinata K, et al. (2006) Uncertainty in treatment of head-and-neck tumors by use of intraoral mouthpiece and embedded fiducials. Int J Radiat Oncol Biol Phys 64:1581–1588
21. Ahn YC, Shimizu S, Shirato H, et al. (2004) Application of real-time tumor-tracking and gated radiotherapy system for unresectable pancreatic cancer. Yonsei Med J 45:584–590
22. Kitamura K, Shirato H, Shimizu S, et al. (2002) Registration accuracy and possible migration of internal fiducial gold marker implanted in prostate and liver treated with real-time tumor-tracking radiation therapy (RTRT). Radiother Oncol 62:275–281
23. Shirato H, Harada T, Harabayashi T, et al. (2003) Feasibility of insertion/implantation of 2.0-mm-diameter gold internal fiducial markers for precise setup and real-time tumor tracking in radiotherapy. Int J Radiat Oncol Biol Phys 56:240–247
24. Imura M, Yamazaki K, Shirato H, et al. (2005) Insertion and fixation of fiducial markers for setup and tracking of lung tumors in radiotherapy. Int J Radiat Oncol Biol Phys 63:1442–1447
25. Shirato H, Oita M, Fujita K, et al. (2004) Three-dimensional conformal setup (3D-CSU) of patients using the coordinate system provided by three internal fiducial markers and two orthogonal diagnostic X-ray systems in the treatment room. Int J Radiat Oncol Biol Phys 60:607–612
26. Shirato H, Suzuki K, Sharp GC, et al. (2006) Speed and amplitude of lung tumor motion precisely detected in four-dimensional setup and in real-time tumour-tracking radiotherapy. Int J Radiat Oncol Biol Phys 64:1229–1236
27. Berbeco R, Nishioka S, Shirato H, et al. (2005) Residual motion of lung tumours in gated radiotherapy with external respiratory surrogates. Phys Med Biol 50:3655–3667
28. Sharp GC, Jiang SB, Shimizu S, et al. (2004) Prediction of respiratory tumour motion for real-time image-guided radiotherapy. Phys Med Biol 49:425–440
29. Shirato H, Seppenwoolde Y, et al. (2004) Intrafractional tumor motion: lung and liver. Semin Radiat Oncol 14:10–18

Clin Exp Metastasis (2007) 24:533–540
DOI 10.1007/s10585-007-9090-x

RESEARCH PAPER

Combination tumor immunotherapy with radiotherapy and Th1 cell therapy against murine lung carcinoma

Hiroshi Yokouchi · Kenji Chamoto · Daiko Wakita · Koichi Yamazaki · Hiroki Shirato · Tsuguhide Takeshima · Hirotoshi Dosaka-Akita · Masaharu Nishimura · Zhang Yue · Hidemitsu Kitamura · Takashi Nishimura

Received: 1 February 2007 / Accepted: 5 July 2007 / Published online: 25 July 2007

Abstract Mice bearing established Lewis lung carcinoma (LLC) expressing model tumor antigen, ovalbumin (OVA) (LLC-OVA) marginally responded to local radiotherapy, but none of the mice was cured. In contrast, treatment of the tumor-bearing mice with intratumoral injection of tumor-specific T helper type 1 (Th1) cells and tumor antigen (OVA) after radiotherapy dramatically prolonged the survival days and induced complete cure of the mice at high frequency (80%). Radiation therapy combined with Th1 cells or OVA alone showed no significant therapeutic activity against LLC-OVA. Such a strong therapeutic activity was not induced by intratumoral injection of Th1 cells plus OVA. Compared with other treatment, radiation therapy combined with Th1 cells and OVA was superior to induce the generation of OVA/H-2^b tetramer$^+$ tumor-specific cytotoxic T lymphocyte (CTL) with a strong cytotoxicity against LLC-OVA in draining lymph node (DLN). Moreover, the combined therapy is demonstrated to inhibit the growth of tumor mass, which grew at contralateral side. These results indicated that radiotherapy combined with Th1 cell/vaccine therapy induced a systemic antitumor immunity. These findings suggested that combination therapy with radiotherapy and Th1 cell/vaccine therapy may become a practical strategy for cancer treatment.

Keywords Draining lymph node · Immunotherapy · Irradiation · Lung cancer · Th1 cells

Hiroshi Yokouchi and Kenji Chamoto are equally contributed.

H. Yokouchi · K. Chamoto · D. Wakita · H. Kitamura · T. Nishimura (✉)
Division of Immunoregulation, Section of Disease Control, Institute for Genetic Medicine, Hokkaido University, N-15, W-7, Kita-ku, Sapporo 060-0815, Japan
e-mail: tak24@igm.hokudai.ac.jp

H. Yokouchi · K. Yamazaki · M. Nishimura
First Department of Medicine, Hokkaido University School of Medicine, Sapporo, Japan

H. Shirato · T. Takeshima
Division of Radiation Oncology, Department of Radiology, Hokkaido University School of Medicine, Sapporo, Japan

H. Dosaka-Akita
Department of Medical Oncology, Hokkaido University Graduate School of Medicine, Sapporo, Japan

Z. Yue
Division of ROYCE' Health Bioscience, Section of Disease Control, Institute for Genetic Medicine, Hokkaido University, Sapporo, Japan

Abbreviations

OVA	Ovalbumin
Th1	T-helper type 1
Ag	Antigen
LLC	Lewis lung carcinoma
CTL	Cytotoxic T lymphocyte
DLN	Draining lymph node
IL	Interleukin
MHC	Major histocompatibility complex
IFN	Interferon
TCR	T cell receptor
MMC	Mitomycin
TIL	Tumor-infiltrating lymphocyte
CT	Computed tomography

Introduction

The role of radiotherapy as a treatment of localized cancer is well established. However, it has been demonstrated that

ionizing radiation can render additional negative impact on immune function of cancer hosts. Irradiation directly induces bone marrow suppression, leading to the cytoreduction of the lymphoid system. The elevated levels of tissue-derived TGF-β [1] and IL-10 [2] by irradiation diminish the activity of T-cell immunity specific for tumor antigens [3]. In contrast, irradiation has been also accepted to create an inflammatory setting in vivo via induction of apoptosis and cell surface molecules or upregulation of MHC and costimulatory molecules, thereby modulated the tumor environment for eliciting potent antitumor immunity [4, 5]. Under these circumstances, various investigators have attempted to optimize the use of radiation by combination with immunological properties such as recombinant cytokines [6], cytokine-gene-transduced tumor or virus vaccinations [7, 8], dendritic cells [9, 10], agonistic anti-CD40 monoclonal antibody [11], ex vivo activated cells from draining lymph node (DLN) [12], adoptive transfer of antigen-specific T cells [13, 14] and peritumoral injection of CpG oligodeoxynucleotide [15, 16] in mouse experimental models.

We have previously demonstrated that T-helper type 1 (Th1)-dominant immunity promotes durable cytotoxic T lymphocyte (CTL) responses and exhibits strong protective antitumor immunity in vivo [17–20]. In the series of our experiments, we demonstrated that the mice bearing MHC-class II-negative E.G7 tumor cells treated with systemic Th1 cell therapy combined with intratumoral injection of tumor antigen were completely cured [20]. However, local treatment would be more suitable for clinical purposes because systemic administration of the Th1 cytokine like IL-2 [21], IFN-γ [22] and whole body irradiation have exhibited significant toxicity, though the treatment effect remained unsatisfactory.

Based on these backgrounds, combinatorial treatment with local irradiation and intratumoral injection of antigen-specific Th1 cells was initiated when established tumors became palpable (8–10 mm in diameter). In this paper, we demonstrated that local radiation therapy greatly enhanced the therapeutic efficacy of Th1 cell/vaccine therapy through the generation of tumor-specific $CD8^+$ CTL.

Materials and methods

Mice

Wild-type C57BL/6 mice were obtained from Charles River Japan (Yokohama, Japan). OT-II T cell receptor (TCR)-transgenic mice, expressing a TCR recognizing the dominant I-A^b-restricted OVA epitope ISQAVHAAHAEINAGR (OVA $_{323-339}$) were kindly provided by F. R. Carbone (University of Melbourne, VIC, Australia). C57BL/6 mice were all female and used at 5–6 weeks of age. All animal experiments were approved by the committee in our animal institute.

Reagents and monoclonal antibodies

Phycoerythrin (PE) conjugated tetramer of H-$2K^b$-restricted OVA $_{257-264}$ (SIINFEKL) molecules (OVA-MHC tetramer) was purchased from MBL (Nagoya, Japan). FITC-labeled CD8 mAb were purchased from BD Pharmingen (San Diego, CA). Anti-CD4 mAb-conjugated microbeads for the MACS system were purchased from Miltenyi Biotec (Bergisch Gladbach, Germany). OVA protein was obtained from SIGMA (St. Louis, MO). IL-12 was kindly donated by Dr. Steven H. Herrmann (Wyeth Research Co Ltd, Cambridge, MA). IL-2 was supplied by Ms. Takuko Sawada (Shionogi Pharmaceutical Institute Co Ltd, Osaka, Japan). Anti-IL-4 mAb (11B11) was purchased from American Type Culture Collection (Rockville, MD). Recombinant IFN-γ was purchased from Pepro Tech EC ltd (London, England). OVA $_{323-339}$ peptide was kindly supplied by Dr. H. Tashiro (Fujiya Co Ltd, Hadano, Japan).

Cell culture

Lewis lung carcinoma (LLC) cell line is a mouse lung carcinoma of C57BL/6 origin. The LLC-OVA cell line was derived from LLC by transfection with chicken OVA cDNA. Cells were cultured in Iscove's Modified Dulbecco's Medium (Invitrogen Corp, Carlsbad, CA) supplemented with 10% fetal bovine serum (Invitrogen Corp), L-glutamine, 25 mM *N*-2-hydroxyethylpiperazine-*N'*-3-propanesulfonic acid (HEPES) buffer, 0.05 mM 2-mercaptoethanol (2-ME), penicillin and streptomycin. To enhance the expression of MHC class I, LLC cells were treated with 10 ng/ml of IFN-γ for 48 h at 37°C and were washed three times with medium before testing by cytotoxicity assays. T cell lymphoma MBL-2 lymphoma was cultured in RPMI1640 medium (SIGMA) supplemented with 10% fetal bovine serum, 2 mM L-glutamine, 0.05 mM 2-ME, HEPES, penicillin and streptomycin. To prepare OT-II mice derived IFN-γ-producing $CD4^+$ T cells (Th1 cells), $CD4^+$ $CD45RB^+$ naïve T cells were isolated from spleen cells from OT-II mice using FACS Vantage (Becton Dickinson, San Jose, CA) as reported previously [23]. Purified $CD4^+CD45RB^+$ cells were stimulated with OVA peptide (5 μg/ml) in the presence of MMC-treated splenocytes from wild-type C57BL/6 mice, anti-IL-4 mAb (50 μg/ml), IL-2 (100 U/ml), IFN-γ (1 ng/ml), and IL-12 (20 U/ml). At 48 h, cells were restimulated with OVA $_{323-339}$ under the same conditions, and used at 9–12 days of culture.

Local irradiation

The mice bearing LLC-OVA were anesthetized, immobilized in a plastic syringe with a hole from which we can pull out the target tumor, and put the mouse under a 8 mm-thick lead shield with a 10 × 10 mm hole. In therapeutic experiments (Figs. 1 and 4), the mouse was locally irradiated with a single dose of 20 Gy (^{60}Co source, Toshiba, Tokyo, Japan, 1 Gy/min) through the hole at Central Institute of Isotope Science, Hokkaido University. In the experiments shown in Figs. 2 and 3, the mouse was locally irradiated with a single dose of 18 Gy (X ray, Toshiba, Tokyo, Japan, 10 Gy/min) through the animal facility of Hokkaido University School of Medicine.

Treatment protocol

Mice were injected intradermally into the right flank at day 0 with 2×10^6 tumor cells per mouse in 150 μl of phosphate-buffered saline (PBS). The mice bearing LLC-OVA were locally irradiated with a single dose of 20 Gy on day 5 when the diameter of inoculated tumor reached around 8–10 mm. Five days after irradiation, the tumor-bearing mice were further treated with intratumoral injection of 2×10^7 OT-II mice-derived Th1 cells with 50 μg OVA antigen in 100 μl of PBS every 2 days for three times. Mice were measured for tumor growth using calipers every other day and tumor volume was calculated by the following formula: tumor volume = 0.4 × length (mm) × [width (mm)]^2 [24]. For contralateral experiments, mice were injected intradermally into both flanks with 2×10^6 LLC-OVA cells each. The right flank of the double tumor-bearing mice were treated with the same therapy as the mice bearing single tumor, and then tumor volume of both tumors was calculated in the same manner above. Experimental groups consisted of five mice/group.

Tetramer staining

Tumor-infiltrating lymphocytes (TILs) were isolated from tumor tissues using protease (DISPASE, Godoshusei Co Ltd, Tokyo, Japan) followed by Percoll (Amersham Biosciences Corp, Piscataway, NJ) gradient method. We slightly modified the use of OVA-MHC tetramer. Briefly, lymphocytes from lymph nodes and tumor tissues were washed with PBS twice, stained with 2 μl OVA -MHC tetramers per 1×10^6 cells and then incubated at 4°C for 15 min. The cells were again washed with PBS. The cells were stained with FITC-conjugated anti-CD8 mAb at 4°C for 15 min, then subjected to the FACS analysis.

Flow cytometry

Detailed procedures for staining and sorting were described previously [18]. Fluorescence data were collected on a FACSCalibur flow cytometer (Becton Dickinson, San Jose, CA), and analyzed using CellQuest software (BD Biosciences, Mountain View, CA).

Cytotoxicity assay

The cytolytic activity of lymphocytes obtained from DLN was assessed in ^{51}Cr release assays as described previously [18]. Tumor-specific cytotoxicity of the cells was determined using LLC-OVA prepared from established tumors as target cells. LLC-OVA tumor burdens isolated from the

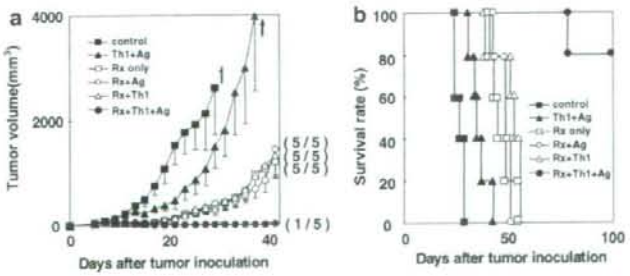

Fig. 1 Local gamma irradiation in combination with intratumoral Th1 cells and antigens eradicate established tumors. LLC-OVA cells (2×10^6) were inoculated intradermally into C57BL/6 mice. When the tumor diameter reached 8–10 mm on day 5, the tumor-bearing mice were treated with various protocols. (**a**) Tumor-bearing mice were treated with PBS (closed square), or local irradiation (Rx: 20 Gy) only (open square), irradiation with intratumoral injection of OVA protein (Ag: 50 μg) (open circle), irradiation with local administration of Th1 cells (2×10^7) (open triangle), Th1 plus Ag with (closed circle) or without (closed triangle) irradiation. The antitumor activity induced by the treatment was determined by measuring tumor size in perpendicular diameters. Tumor volume was calculated as described in "Material and methods." The fractional numbers in parenthesis indicate dead mice/total mice within 100 days after tumor inoculation. (**b**) Survival of mice following various protocols is shown. Similar results were obtained in three separate experiments. Data are presented as the mean ± SE

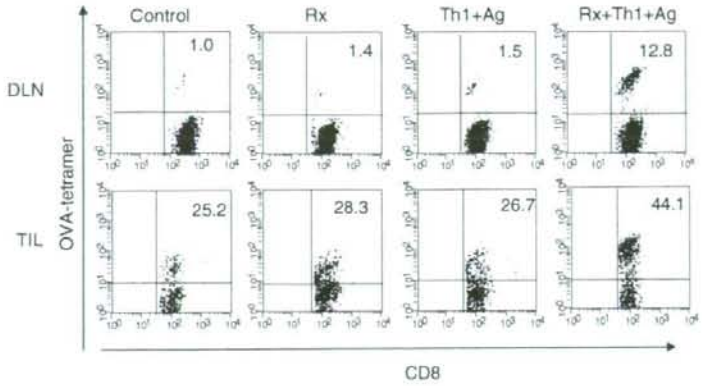

Fig. 2 OVA-MHC tetramer$^+$ CTLs were efficiently mobilized into both DLNs and tumor tissues from the mice treated with local irradiation and intratumoral administration of Th1 cells plus antigens. LLC-OVA cells (2×10^6) were inoculated intradermally into C57BL/6 mice and the tumor-bearing mice were treated with various protocols. The tumor was locally irradiated (18 Gy) on day 5, and Th1 cells (2×10^7) with antigens (50 μg) were administered intratumorally on day 10. DLNs and TILs obtained from the mice treated with indicated therapy on day 18 were labeled with PE-conjugated OVA-MHC tetramer, followed by staining with FITC-conjugated anti-CD8 mAb. About 5,000 CD8$^+$ T cells in DLN and 3,000 CD8$^+$ T cells in tumor were acquired and analyzed. The numbers indicate the percentage of tetramer-positive cells in the CD8$^+$ population. Similar results were obtained in three separate experiments

mice 10 days after inoculation in C57BL/6 mice were minced without using digestive enzymes and incubated on 10 cm plate for 2 h at 37°C, then the supernatant was removed by gently pipetting. Residual adherent cells were harvested by vigorous pipetting and used as targets. As a control, MBL-2 and IFN-γ pre-treated LLC cell lines cultivated in vitro were used. We had already confirmed the expression of MHC-class I on MBL-2 cell lines cultivated in vitro (data not shown). We also had found upregulated expression of MHC-class I molecules on LLC-OVA cells ex vivo, though the expression of in vitro LLC and LLC-OVA cell lines without IFN-γ treatment are extremely weak (data not shown). All cell lines were MHC-class II negative despite of pretreatment with IFN-γ. Pre-labeling of effector cells with OVA-MHC tetramer was used for the purpose of detecting MHC-restricted and antigen-specific cytotoxicities [25]. Briefly, whole DLN cells from the mice treated with combination therapy were labeled with 2 μl OVA-MHC tetramer per 1×10^6 cells and then incubated at 4°C for 15 min. The assay was carried out in triplicate samples at the indicated effector:target ratios (E:T). The percentage of cytotoxicity was calculated as described previously [18].

Results

Local irradiation combined with intratumoral injection of tumor-specific Th1 cells and model tumor antigen induce significant eradication of a well-established LLC-OVA

C57BL/6 mice bearing with lung carcinoma (LLC-OVA) expressing OVA as model tumor antigen were treated with local irradiation (Rx) in combination with intratumoral injection of OVA-specific Th1 cells and OVA model tumor antigens (Ag) (Rx + Th1 + Ag; combination therapy, hereafter). The growth of LLC-OVA was not inhibited by intratumoral injection of Th1 cell therapy alone or antigen alone (data not shown). In three radiotherapy groups (Rx alone, Rx + Ag, Rx + Th1), marginal inhibition of tumor growth was induced. However, none of the mice was cured from tumor. On the other hand, 80% of tumor-bearing mice treated with combination therapy were completely cured from tumor and only one of five mice treated with the combination therapy exhibited the recurrence of tumor growth on day 33 (Fig. 1a). We initially performed the dose searching study of irradiation with fixed dose of Th1 cells and antigen, but none of the treated mice was completely cured from tumor with the irradiation dose under 20 Gy (data not shown). This high dose of local irradiation was well tolerated by virtue of a complete shielding of whole body except for tumor site. In parallel with these results, all the treated mice except for combination therapy died by day 60, while combination therapy induced long-term (day 100) eradication of 80% of the mice (Fig. 1b). These results suggested that combination therapy with irradiation and Th1 cells with antigens induce efficient tumor elimination, leading to long-term survival with acceptable feasibility.

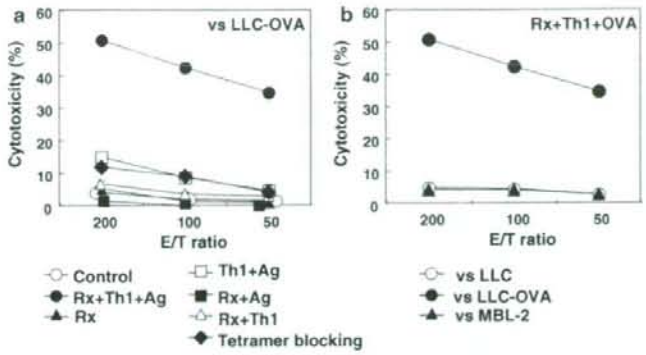

Fig. 3 Tumor-specific CTL activity is augmented by local irradiation in combination with intratumoral Th1 administration and antigens. LLC-OVA cells (2×10^6) were inoculated intradermally into C57BL/6 mice. When the tumor diameter reached 8–10 mm on day 5, the tumor-bearing mice were treated with various protocols. The cells in DLN from the mice treated with various treatments as indicated were harvested on day 18. The harvested cells were used without ex vivo culture in 4 h-^{51}Cr release assay. (**a**) Cytolytic activities by whole DLN cells from the mice treated with indicated protocols were tested against LLC-OVA. In tetramer blocking assay, whole DLN cells prepared from combination therapy were labeled with OVA—MHC tetramer and the cytotoxic activities were tested against LLC-OVA. (**b**) CTL activities by whole DLN cells from the mice treated with combination therapy were tested against LLC-OVA (closed circle), LLC (open circle) and MBL-2 (closed triangle). Similar results were obtained in three separate experiments. The bar means ± SE of duplicated samples

Combination tumor immunotherapy with radiotherapy and Th1 cell therapy induces tumor-specific CD8$^+$ T effector cells and systemic antitumor immunity.

The frequency of OVA-MHC tetramer$^+$ CD8$^+$ CTL generation in DLN and tumor tissue of tumor-bearing mice was examined 48 h after second treatment with Rx, Th1 + Ag or Rx + Th1 + Ag. As shown in Fig. 2, both DLN and TIL obtained from mice treated with Rx + Th1 + Ag revealed highest accumulation of tetramer$^+$ CTL compared with other treatment. The frequencies of tetramer$^+$ CD8$^+$ T cells in both draining lymph nodes (DLNs) and tumor tissues obtained from the mice treated with Th1 alone and antigen alone were the same as those from control mice, and the cells from the mice treated with Rx + Ag and Rx + Th1 groups were quite similar to those from Rx alone (data not shown). To investigate whether the lymphocytes in DLN from the mice treated with combination therapy contain cytotoxic effectors, we examined their cytotoxicity against LLC-OVA. As shown in Fig. 3a, whole DLN cells derived from mice treated with the combination therapy exhibited highest cytotoxicity against LLC-OVA compared with those derived from mice treated with none, Rx, Rx + Th1, Rx + Ag or Th1 + Ag. It was also demonstrated that the DLN cells from mice treated with the combination therapy showed tumor-specific cytotoxicity against LLC-OVA but not against LLC, MBL-2 cells (Fig. 3b). Moreover as shown in Fig. 3a, OVA-MHC-tetramer treatment inhibited CD8$^+$ CTL-mediated cytotoxicity against LLC-OVA in the group of combination therapy, which we termed tetramer-blocking assay [25]. These findings demonstrated that the combination therapy augmented the recruitment of antigen-specific CD8$^+$ T cells, which surely recognized the OVA antigenic peptide bound to MHC Class I (H-2^b), into DLNs and TILs to eradicate tumor tissue in vivo.

Clinical impact of immunotherapy is its possibility of inducing systemic therapeutic effect. To estimate this, we made a double tumor-bearing mouse model. Right flank of the double tumor-bearing mice were treated with the same therapy as the mice bearing single tumor (Fig. 4a), and we examined the growth of contralateral untreated tumor, which was distant from the treated one. Combination therapy significantly suppressed the growth of uninjected tumors. This effect was not found in mice treated with other regimens (Fig. 4b). These results suggest that this combined therapy can establish strong systemic antitumor immunity and it can be applied for the metastatic therapy model.

Discussion

We demonstrated the induction of high complete cure rate of mice bearing mouse lung carcinoma by combined local irradiation and intratumoral administration of antigen-specific Th1 cells with cognate antigen proteins.

Though co-administration of 50 μg OVA antigens was eventually required for the tumor eradication in this treatment, we did not eradicate LLC-OVA cells by using Th1 cells and 200 μg OVA antigens without irradiation (data not shown). These results suggest that irradiation can reduce the requirement of exogenous administration of

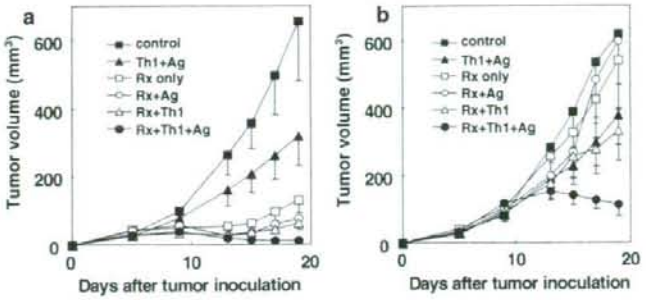

Fig. 4 Local irradiation in combination with Intratumoral administration of Th1 cells and antigens mediates significant regression of contralateral untreated tumors. Mice were injected intradermally with 2×10^6 LLC-OVA cells each in both flanks. On day 5 when the both tumors' diameter reached 8–10 mm, local irradiation only (open square), or irradiation with local administration of antigen (50 μg) (open circle), or irradiation with local administration of Th1 cells (2×10^7) (open triangle), or Th1 plus OVA antigen with (closed circle) or without (closed triangle) irradiation were treated into established tumors in right flank same as the protocol in Fig. 1. The growth of treated tumor in right flanks and untreated tumor in left flanks were monitored as shown in (**a**) and (**b**), respectively. Similar results were obtained in two separate experiments. Data are presented as the mean ± SE

antigens for eliciting antitumor immunity. Recently, a study was reported on the combination of CpG and radiation, showing that CpG was more effective in enhancing the effect of fractionated than single-dose radiation in a mouse model [16]. This efficient protocol seems practical in clinics because the fractionated schedule is commonly used in clinical radiotherapy. Thus, it should be in consideration for the combination of fractionated radiotherapy with Th1 cells in our study. This strategy might enable us to thoroughly reduce exogenous antigens and induce more promising antitumor efficacy.

Recently it has been demonstrated that the frequency of antigen-MHC tetramer is not correlated with the clinical responses [26, 27]. We actually detected tetramer$^+$ CD8$^+$ T cells in DLNs and tumor tissues from the mice of the groups that failed to cure. However, the frequency of tetramer$^+$ CD8$^+$ T cells in DLNs from the mice treated with combination therapy was the highest and significant tumor growth inhibition and high survival rate were observed. Moreover the DLN cells of the mice treated with this therapy killed tumors strongly ex vivo and their cytotoxicity was antigen-specific (Fig. 3). Therefore, this combination therapy enabled us to overcome the tumor defense system with less productivity of immunosupressive regulatory population or with alteration of their tolerized phenotype into activated states. It has been well accepted that generation of antigen-specific Th1 cells is quite difficult and time-consuming. However, we developed an efficient protocol for preparing mouse and human antigen-specific Th1 cells from nonspecifically activated Th1 cells after retroviral transfer of TCR-α and TCR-β genes [28] or lentiviral mediated chimeric immune receptor gene-encoding [29]. We could demonstrate that these antigen-specific artificial Th1 cells expanded in vitro was beneficial for the treatment of cognate tumors in vivo.

We have already established the direct delivery system by which we could mobilize various interventional devises to small peripheral pulmonary lesions of less than 20 mm in diameter using ultrathin bronchoscope under computed tomography (CT) guidance and virtual bronchoscopic navigation [30]. We presume that this method is applicable for the present therapeutic design using intratumoral administration of Th1 cells and/or antigens. Moreover, the radiologists in our university hospital have developed small-volume hypofractionated image-guided radiotherapy without a need for breath control [31]. By this method, the high dose nearly 12 Gy at a time can be applicable for lung cancer patients. They and our colleagues showed its safety and efficiency [32–34]. We showed in this article that the combined therapy led to the induction of systemic antitumor immunity (Fig. 4). Thus we hope the combination therapy could apply to lung metastasis. Although LLC-OVA did not metastasize to other organs, we are now exploring the lung metastatic mice model using other cancers such as B16 melanoma to prove the systemic anti-metastatic efficacy of combined radiotherapy with Th1 cell therapy.

Though further work is required to increase our understanding of the tumor eradication mechanism and to investigate the best protocol design, we hope the results of this experiment will be a rationale study for future clinical trials. Combined radiotherapy with Th1 cell therapy may become a next practical strategy against advanced cancer patients.

Acknowledgements We thank Dr. Steven H. Herrmann (Wyeth Research Co Ltd, Cambridge, MA) and Ms Takuko Sawada (Shionogi Pharmaceutical Institute Co, Osaka, Japan) for their kind donations of IL-12 and IL-2, respectively. We are grateful to Ms Takae Ohyama for her kindly support of breading mice in the animal institute of Hokkaido University. We thank Dr. Takashige Abe for technical

advice of irradiation. This study is supported in part by a Grant-in Aid from the Ministry of Education Culture, Sports, Science, and Technology, a Grant-in-Aid for Scientific Research on priority Areas, a Grant-in-Aid for Immunological Surveillance and its Regulation, a Grant-in-Aid for ministry of Education, Culture Sports, Science and Technology Cancer Translational Research Project and a Grant-in-Aid for Scientific Research (A).

References

1. Canney PA, Dean S (1990) Transforming growth factor beta: a promoter of late connective tissue injury following radiotherapy? Br J Radiol 63(752):620–623
2. Broski AP, Halloran PF (1994) Tissue distribution of IL-10 mRNA in normal mice. Evidence that a component of IL-10 expression is T and B cell-independent and increased by irradiation. Transplantation 57(4):582–592
3. Horwitz DA, Zheng SG, Gray JD (2003) The role of the combination of IL-2 and TGF-β or IL-10 in the generation and function of $CD4^+$ $CD25^+$ and $CD8^+$ regulatory T cell subsets. J Leuko Biol 74(4):471–478
4. Friedman EJ (2002) Immune modulation by ionizing radiation and its implications for cancer immunotherapy. Curr Pharm Des 8(19):1765–1780
5. Garnett CT, Palena C, Chakarborty M, Tsang KY, Schlom J, Hodge JW (2004) Sublethal irradiation of human tumor cells modulate phenotype resulting in enhanced killing by cytotoxic T lymphocytes. Cancer Res 64(21):7985–7994
6. Dybal EJ, Haas GP, Maughan RL, Sud S, Pontes JE, Hillman GG (1992) Synergy of radiation therapy and immunotherapy in murine renal cell carcinoma. J Urol 148(4):1331–1337
7. Lumniczky K, Desaknai S, Mangel L, Szonde B, Hamada H, Hidvegi EJ, Safrany G (2002) Local tumor irradiation augments the antitumor effect of cytokine-producing autologous cancer cell vaccines in a murine glioma model. Cancer Gene Ther 9(1):44–52
8. Hillman GG, Slos P, Wang Y, Wright JL, Layer A, De Meyer M, Yudelev M, Che M, Forman JD (2004) Tumor irradiation followed by intratumoral cytokine gene therapy for murine renal adenocarcinoma. Cancer Gene Ther 11(1):61–72
9. Nikitina EY, Gabrilovich DI (2001) Combination of γ-irradiation and dendritic cell administraion induces a potent antitumor response in tumor-bearing mice: approach to treatment of advanced stage cancer. Int J Cancer 94(6):825–833
10. Teitz-Tennenbaum S, Li Q, Rynkiewicz S, Ito F, Davis MA, McGinn CJ, Chang AE (2003) Radiotherapy potentiates the therapeutic efficacy of intratumoral dendritic cell administration. Cancer Res 63(23):8466–8475
11. Honeychurch J, Glennie MJ, Johnson PWM, Illidge TM (2003) Anti-CD40 monoclonal antibody therapy in combination with irradiation results in a CD8 T-cell-dependent immunity to B-cell lymphoma. Blood 102(4):1449–1457
12. Plautz GE, Inoue M, Shu S (1996) Defining the synergistic effects of irradiation and T-cell immunotherapy for murine intracranial tumors. Cell Immunol 171(2):277–284
13. Ganss R, Ryschich E, Klar E, Arnold B, Hammerling GJ (2002) Combination of T-cell therapy and trigger of inflammation induces remodeling of the vasculature and tumor eradication. Cancer Res 62(5):1462–1470
14. Cao ZA, Daniel D, Hanahan D (2002) Sub-lethal radiation enhances anti-tumor immunotherapy in a transgenic mouse model of pancreatic cancer. BMC cancer 2:11
15. Milas L, Mason KA, Ariga H, Hunter N, Neal R, Valdecanas D, Krieg AM, Whisnant JK (2004) CpG oligodeoxynucleotide enhances tumor response to radiation. Cancer Res 64(15):5074–5077
16. Mason KA, Ariga H, Neal R, Valdecanas D, Hunter N, Krieg AM, Whisnant JK, Milas L (2005) Targeting toll-like receptor 9 with CpG oligodeoxynucleotides enhances tumor response to fractionated radiotherapy. Clin Cancer Res 11(1):361–369
17. Nishimura T, Iwakabe K, Sekimoto M, Ohmi Y, Yahata T, Nakui M, Sato T, Habu S, Tashiro H, Sato M, Ohta A (1999) Distinct role of antigen-specific T helper type 1 (Th1) and Th2 cells in tumor eradication in vivo. J Exp Med 190(5):617–628
18. Nishimura T, Nakui M, Sato M, Iwakabe K, Kitamura H, Sekimoto M, Ohta A, Koda T, Nishimura S (2000) The critical role of Th1-dominant immunity in tumor immunology. Cancer Chemother Pharmacol 46(Suppl):S52–61
19. Chamoto K, Kosaka A, Tsuji T, Matsuzaki J, Sato T, Takeshima T, Iwakabe K, Togashi Y, Koda T, Nishimura T (2003) Critical role of the Th1/Tc1 circuit for the generation of tumor-specific CTL during tumor eradication in vivo by Th1-cell therapy. Cancer Sci 94(10):924–928
20. Ikeda H, Chamoto K, Tsuji T, Suzuki Y, Wakita D, Takeshima T, Nishimura T (2004) The critical role of type-1 innate and acquired immunity in tumor immunotherapy. Cancer Sci 95(9):697–703
21. Davis ID, Jefford M, Parente P, Cebon J (2003) Rational approaches to human cancer immunotherapy. J Leuko Biol 73(1):3–29
22. Schiller JH, Pugh M, Kirkwood JM, Karp D, Larson M, Borden E (1996) Eastern cooperative group trial of interferon gamma in metastatic melanoma: an innovative study design. Clin Cancer Res 2(1):29–36
23. Ohta A, Sato N, Yahata T, Ohmi Y, Santa K, Sato T, Tashiro H, Habu S, Nishimura T (1997) Manipulation of Th1/Th2 balance in vivo by adoptive transfer of antigen-specific Th1 or Th2 cells. J Immunol Methods 209(1):85–92
24. Ohta S, Tsukamoto H, Watanabe K, Makino K, Kuge S, Hanai N, Habu S, Nishimura T (1995) Tumor-associated glycoantigen, sialyl Lewis (a) as a target for bispecific antibody-directed adoptive tumor immunotherapy. Immunol Lett 44(1):35–40
25. Yokouchi H, Chamoto K, Wakita D, Noguchi D, Yamazaki K, Dosaka-Akita H, Nishimura M, Ikeda H, Nishimura T (2006) Tetramer-blocking assay for defining antigen-specific cytotoxic T lymphocytes using peptide-MHC tetramer. Cancer Sci 97(2):148–154
26. Lee PP, Yee C, Savage PA, Fong L, Brockstedt D, Weber JS, Johnson D, Swetter S, Thompson J, Greenberg PD, Roederer M, Davis MM (1999) Characterization of circulating T cells specific for tumor-associated antigens in melanoma patients. Nature Med 5(6):677–685
27. Lee KH, Wang E, Nielsen MB Wunderlich J, Migneles S, Connors M, Steinberg SM, Rosenberg SA, Marincola FM (1999) Increased vaccine-specific T cell frequency after peptide-based vaccination correlates with increased susceptibility to in vitro stimulation but does not lead to tumor regression. J Immunol 163(11):6292–6300
28. Chamoto K, Tsuji T, Funamoto H, Kosaka A, Matsuzaki J, Sato T, Abe H, Fujio K, Yamamoto K, Kitamura T, Takeshima T, Togashi Y, Nishimura T (2004) Potentiation of tumor eradication by immunotherapy with T-cell receptor gene-transduced T-helper type 1 cells. Cancer Res 64(4):386–390
29. Gyobu H, Tsuji T, Suzuki Y, Ohkuri T, Chamoto K, Kuroki M, Miyoshi H, Kawarada Y, Kato H, Takeshima T, Nishimura T (2004) Generation and targeting of human tumor-specific Tc1 and Th1 cells transduced with a lentivirus containing a chimeric immunoglobulin T-cell receptor. Cancer Res 64(4):1490–1495
30. Shinagawa N, Yamazaki K, Onodera Y, Miyasaka K, Kikuchi E, Dosaka-Akita H, Nishimura M (2004) CT-guided transbronchial

biopsy using an ultrathin bronchoscope with virtual bronchoscopic navigation. Chest 125(3):1138–1143
31. Shirato H, Shimizu S, Shimizu T, Nishioka T, Miyasaka K (1999) Real-time tumour-tracking radiotherapy. Lancet 353(9161): 1331–1332
32. Fukumoto S, Shirato H, Shimizu S, Ogura S, Onimaru R, Kitamura K, Yamazaki K, Miyasaka K, Nishimura M, Dosaka-Akita H (2002) Small-volume image-guided radiotherapy using hypofractionated coplanar, and noncoplanar multiple fields for patients with inoperable stage I nonsmall cell lung carcinomas. Cancer 95(7):1546–1553
33. Harada T, Shirato H, Ogura S, Oizumi S, Yamazaki K, Shimizu S, Onimaru R, Miyasaka K, Nishimura M, Dosaka-Akita H (2002) Real-time tumor-tracking radiation therapy for lung carcinoma by the aid of insertion of a gold marker using bronchofiberscopy. Cancer 95(8):1720–1727
34. Onimaru R, Shirato H, Shimizu K, Kitamura K, Xu B, Fukumoto S, Chang TC, Fujita K, Oita M, Miyasaka K, Nishimura M, Dosaka-Akita H (2003) Tolerance of organs at risk in small-volume hypofractionated, image-guided radiotherapy for primary and metastatic lung cancers. Int J Rad Oncol Biol Phys 56(1):126–135

手術手技・周術期管理

斜台部腫瘍摘出における経鼻孔内視鏡手術の経験
—術式の工夫—

斎藤佑規　土谷大輔　櫻田　香
佐藤慎哉　黒木　亮　嘉山孝正

Technical Notes on Endoscopic Transnasal Transsphenoidal Approach for Clival Tumor

by
Yuki Saito, M.D., Daisuke Tsuchiya, M.D., Kaori Sakurada, M.D., Shinya Sato, M.D., Akira Kuroki, M.D., and Takamasa Kayama, M.D.
from
Department of Neurosurgery, Yamagatga University Faculty of Medicine

Although there are various operative approaches for clival tumors, a transsphenoidal approach is one of choices when the main tumor extension is in an anterior-posterior direction with a slight lateral extension. However, this approach sometimes provides only narrow and deep operative fields. The recent development of a neuroendoscope and neuronavigation system allow for a wide operative field and easy identification of the surrounding important structures. As a result, an endoscopic transsphenoidal approach is now quite an effective approach for clival tumors. In this report, we discribe the effectiveness, technical problems, and solution of this approach based on our experience with a chondrosarcoma that was removed by endoscopic transsphenoidal approach.

(Received March 22, 2007; accepted May 25, 2007)

Key words : chondrosarcoma, clival tumor, endoscope, neuronavigation, transsphenoidal approach
Jpn J Neurosurg (Tokyo) 17 : 50-54, 2008

緒　言

頭蓋底の chondrosarcoma は浸潤性に発育することが多く，外科的切除は，transbasal approach，transmaxillary approach，transoral approach，transfacial approach，subtemporal approach，transsphenoidal approach など，多くの手術アプローチが報告されているが[1)7)9)]，いずれのアプローチでも広い術野を得ることは困難で，また周囲に存在する重要血管や脳神経が術野を制限するので，不十分な切除に終わることが少なくない[3)6)]．

斜台部腫瘍に対する transsphenoidal approach[4)10)]は，1960 年代[2)]から用いられているが，当時の手術用顕微鏡では視野の確保に制限があり，また閉創の困難さから髄液漏が問題となった[10)]．そのため，chordoma の手術アプローチとしてはあまり普及しなかった．今回は，最新の神経内視鏡システムを駆使し，transnasal transsphenoidal approach にて摘出を行った chondrosarcoma の 1 例を経験したので，内視鏡手術の有用性と限界について，われわれが行った技術的工夫を中心に本症例の手術に対して報告する．

山形大学医学部脳神経外科／〒990-9585 山形市飯田西 2-2-2〔連絡先：嘉山孝正〕
Address reprint requests to: Takamasa Kayama, M.D., Department of Neurosurgery, Yamagata University Faculty of Medicine, 2-2-2 Iida-nishi, Yamagata-shi, Yamagata 990-9585, Japan